Nonsymmorphic cubic Dirac point and crossed nodal rings across the ferroelectric phase transition in LiOsO_{3}

Wing Chi Yu, Xiaoting Zhou, Feng-Chuan Chuang, Shengyuan A. Yang, Hsin Lin, and Arun Bansil

Nonsymmorphic cubic Dirac point and crossed nodal rings across the ferroelectric phase transition in LiOsO₃

Wing Chi Yu[*],[1] Xiaoting Zhou[*],[1, 2, †] Feng-Chuan Chuang,[3] Shengyuan A. Yang,[4, ‡] Hsin Lin,[1, 5, 6, §] and Arun Bansil[7]

[1]*Center for Advanced 2D Materials and Graphene Research Center, National University of Singapore, Singapore 117546, Singapore*
[2]*Physics Division, National Center for Theoretical Science, Hsinchu 30013, Taiwan*
[3]*Department of Physics, National Sun Yat-Sen University, Kaohsiung 804, Taiwan*
[4]*Research Laboratory for Quantum Materials, Singapore University of Technology and Design, Singapore 487372, Singapore*
[5]*Department of Physics, National University of Singapore, Singapore 117546, Singapore*
[6]*Institute of Physics, Academia Sinica, Taipei 11529, Taiwan*
[7]*Department of Physics, Northeastern University, Boston, Massachusetts 02115, USA*

Crystalline symmetries can generate exotic band-crossing features, which can lead to unconventional fermionic excitations with interesting physical properties. We show how a cubic Dirac point—a four-fold-degenerate band-crossing point with cubic dispersion in a plane and a linear dispersion in the third direction—can be stabilized through the presence of a nonsymmorphic glide mirror symmetry in the space group of the crystal. Notably, the cubic Dirac point in our case appears on a threefold axis, even though it has been believed previously that such a point can only appear on a sixfold axis. We show that a cubic Dirac point involving a threefold axis can be realized close to the Fermi level in the non-ferroelectric phase of LiOsO₃. Upon lowering temperature, LiOsO₃ has been shown experimentally to undergo a structural phase transition from the non-ferroelectric phase to the ferroelectric phase with spontaneously broken inversion symmetry. Remarkably, we find that the broken symmetry transforms the cubic Dirac point into three mutually-crossed nodal rings. There also exist several linear Dirac points in the low-energy band structure of LiOsO₃, each of which is transformed into a single nodal ring across the phase transition.

I. INTRODUCTION

In the past decade, the study of topological phases of matter has become one of the most active areas of research in condensed matter physics[1–4]. Extending the earlier work on gapped topological phases, such as topological insulators[5–16] and topological superconductors[17–27], the focus has shifted recently to gapless phases, especially the so-called topological semimetals (TSMs)[28–33].

TSMs are characterized by protected band-crossings in momentum space, which can be zero-dimensional nodal points or one-dimensional nodal lines. Around these band-crossings, electrons behave drastically differently from the conventional Schrödinger fermions. For example, the low-energy electrons in three-dimensional (3D) Dirac[34–38] and Weyl semimetals[39–42] resemble the relativistic Dirac and Weyl fermions with linear dispersion, allowing investigation of related exotic phenomena, which have previously belonged to the domain of high-energy physics, in a desktop materials setting. In fact, the family of nodal-line semimetals[43–55] harbors an even richer topological structure, and supports nodal chains[56,57], crossing nodal lines[58–60] as well as Hopf links[61–66], which have no counterparts in high-energy physics. In addition to these novel bulk fermionic excitations, TSMs also possess exotic topological surface states in the form of Fermi arcs in Dirac/Weyl semimetals and drumhead surface states in nodal-loop semimetals[27,32,39].

Nonsymmorphic crystalline symmetries, i.e. symmetries which involve a fractional lattice translation, can generate TSMs with exotic type of band crossing features. For example, a glide mirror or a two-fold screw axis can give rise to an hourglass dispersion[67], hourglass loop/chain[54–57], and 2D spin-orbit Dirac points[68,69], which are robust against spin-orbit coupling (SOC) effects.

Here, we show that the glide mirror symmetry, combined with symmorphic three-fold rotation, inversion, and time-reversal symmetries, can generate a cubic Dirac point. This cubic Dirac point is four-fold degenerate with an associated band dispersion, which is cubic in a plane and linear in the third direction normal to the plane. Notably, as a result of the nonsymmorphic symmetry, the cubic Dirac point here appears on a threefold axis, even though it has been believed previously that such a point can only appear on a sixfold axis[70,71]. We further show that when the inversion symmetry is broken, this cubic Dirac point transforms into three crossed nodal rings.

Through first-principles electronic structure computations, we show that LiOsO₃ provides a materials platform for realizing the novel topological physics outlined in the preceding paragraph. LiOsO₃ is the first example of a ferroelectric metal[72]. In a recent experiment, Shi *et al.* report that LiOsO₃ undergoes a ferroelectric phase transition at a critical temperature $T^* \approx 140$ K[73], at which the material transforms from a centrosymmetric $R\bar{3}c$ structure to a non-centrosymmetric $R3c$ structure, while remaining metallic. LiOsO₃ thus realizes the scenario proposed in Ref.[72]. Notably, a related material,

HgPbO$_3$, has been suggested recently to host a ferroelectric Weyl semi-metal phase[74].

Our analysis shows that the non-ferroelectric $R\bar{3}c$ structure satisfies the symmetry requirements for hosting a cubic Dirac point. Also, when the inversion symmetry breaks at the ferroelectric transition, we find that the cubic Dirac point gives rise to three crossed nodal rings in the ferroelectric $R3c$ structure. The low-energy band structure of LiOsO$_3$ further shows the presence of several linear Dirac nodes, and we show that these nodes turn into nodal loops during the ferroelectric phase transition. Our study thus not only discovers a new mechanism for generating a cubic Dirac point, but it also offers a promising new materials platform for exploring the interplay between structural transitions, ferroelectricity, and novel topological fermions.

II. COMPUTATIONAL METHODS

Our *ab-initio* calculations were performed by using the all-electron full-potential linearized augmented plane-wave code WIEN2k[75]. Generalized gradient approximation (GGA) of Perdew, Burke and Ernzerhof (PBE)[76] was employed for the exchange-correlation potential. Experimental lattice constants[73] were used in the calculations and the internal structure was optimized. The self-consistent iteration process was repeated until the charge, energy and force converged to less than 0.0001e, 0.00001 Ry, and 1 mRy/a.u, respectively. SOC was included by using the second variational procedure[77]. The muffin-tin radii were set to 1.47, 1.84, and 1.51 a.u. for the Li, Os, and O atoms, respectively. $R_{\mathrm{MT}}^{\mathrm{min}}K_{\mathrm{max}} = 7$ and a k-point mesh of 4000 in the first Brillouin zone were used. An effective tight-binding model was constructed via projection onto the Wannier orbitals[78–82] for carrying out topological analysis of the electronic spectrum.We used the Os d orbitals without performing the maximizing localization procedure. Surface states were obtained using the surface Green's function technique[83] applied on a semi-infinite slab.

III. CRYSTAL STRUCTURE AND SYMMETRY

The non-ferroelectric phase of LiOsO$_3$ has a rhombohedral structure with space group $R\bar{3}c$ (No.167) [Fig. 1(a)]. The Os atom is located at the center between two Li atoms and also at the symmetric position of two O planes, which preserves inversion symmetry $\mathcal{P}$. Upon lowering the temperature below T^*, the two Os atoms are displaced along the [111] direction, resulting in the loss of inversion center [Fig. 1(b)][73]. The crystal symmetry is thus lowered to $R3c$ (No.161) in the ferroelectric phase.

We emphasize that the key physics underlying the cubic Dirac point and its transformations in LiOsO$_3$ is controlled by symmetry, and not by the details of the specific material involved. The important symmetries are as fol-
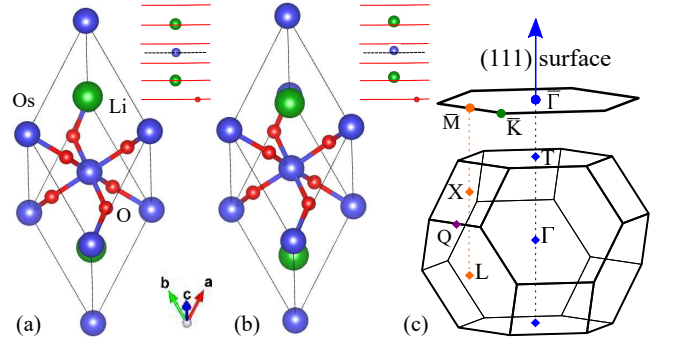

FIG. 1: Crystal structures of LiOsO$_3$ (a) The non-ferroelectric phase and (b) the ferroelectric phase. The insets are schematic drawings of the oxygen planes (red lines) and the location of the Os and Li atoms relative to these planes. (c) Brillouin zone (BZ) of LiOsO$_3$ and the projected (111) surface BZ.

lows. The $R\bar{3}c$ space group of the non-ferroelectric phase can be generated by three symmetry elements: the inversion $\mathcal{P}$, the three-fold rotation along [111]-direction (z-axis) c_{3z}, and the glide mirror with respect to the ($\bar{1}10$) plane (xz-plane) $\widetilde{M_y} = \{M_y|\frac{1}{2}\frac{1}{2}\frac{1}{2}\}$, which is a nonsymmorphic symmetry. In the ferroelectric phase, when $\mathcal{P}$ is broken, the generators of the remaining $R3c$ space group reduce to c_{3z} and $\widetilde{M_y}$ only. Lattices in both phases are bipartite: there are two sublattices (denoted as A and B) with a relative displacement of $(\frac{1}{2}, \frac{1}{2}, \frac{1}{2})$. $\mathcal{P}$ and $\widetilde{M_y}$ map between the two sublattices ($A \leftrightarrow B$), whereas C_{3z} maps within each sublattice ($A(B) \leftrightarrow A(B)$). The system preserves the time-reversal symmetry $\mathcal{T}$, since no magnetic ordering has been observed in either phase[73].

IV. BAND STRUCTURES WITHOUT SOC

Without the SOC, the band structures of non-ferroelectric and ferroelectric phases of LiOsO$_3$ are similar as seen in Fig. 2. Both phases exhibit two-fold degenerate (four-fold if spin-degeneracy is counted) nodal lines passing through the L and T points of the BZ perpendicular to the glide mirror planes. These features of the band structure can be understood by noting that the L and T are time-reversal invariant momentum (TRIM) points, which also reside on the glide mirror planes $\widetilde{M_i}$ ($i = 1, 2, 3$) (the other two glide mirrors are related to $\widetilde{M_y}$ by C_{3z}), see Fig. 1(c). It is easily seen that the line passing through an L point and normal to the corresponding mirror plane $\widetilde{M_i}$ is invariant under the anti-unitary symmetry operation $\mathcal{T}\widetilde{M_i}$, so that

$$(\mathcal{T}\widetilde{M_i})^2 = e^{-ik_z^L} = -1, \tag{1}$$

where we have used $\mathcal{T}^2 = +1$ for a spinless system and k_z^L is the k_z-component of L. The $\mathcal{T}\widetilde{M_i}$ symmetry thus guarantees a two-fold Kramers-like degeneracy on this
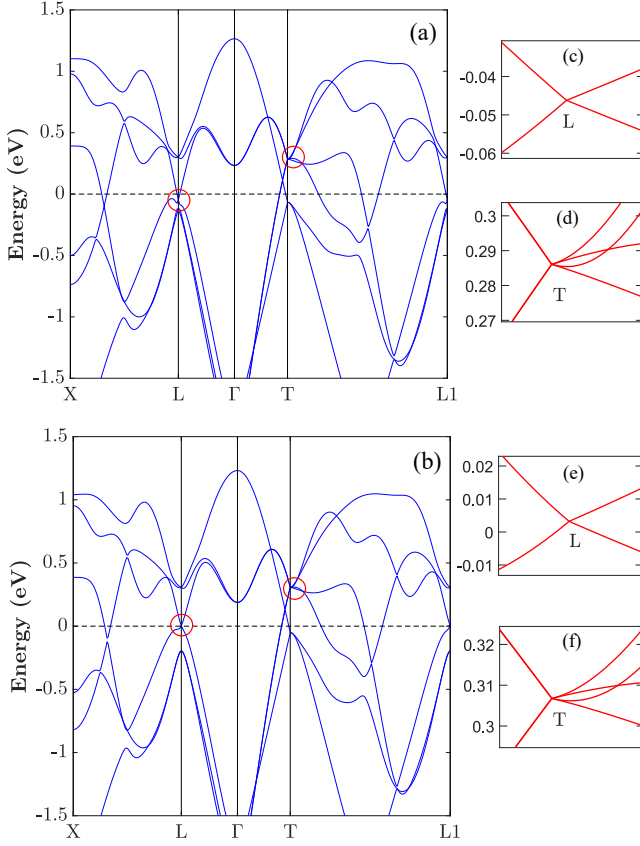
FIG. 2: Electronic band structure of LiOsO$_3$ in the absence of SOC for (a) the non-ferroelectric phase and, (b) the ferroelectric phase. (c)-(f) Zoom-in images of the band crossings at the L and T symmetry points marked by red circles in (a) and (b).

line. A similar analysis applies to the T point: Since T lies on the intersection of three glide mirrors, three such nodal lines pass through T. Moreover, since $\widetilde{M}_{i+1} = C_{3z}\widetilde{M}_i C_{3z}^{-1}$, $[C_{3z}, \widetilde{M}_y] \neq 0$, which leads to $[\widetilde{M}_i, \widetilde{M}_{j\neq i}] \neq 0$. For an eigenstate $|\psi_0\rangle$ at T, the three states $|\psi_{i=1,2,3}\rangle = \mathcal{T}\widetilde{M}_i|\psi_0\rangle$ must be orthogonal to each other, indicating a four-fold (eight-fold if counting spin) degeneracy at T. This analysis is in accord with our DFT band structure results.

V. BAND STRUCTURES WITH SOC

A. Non-ferroelectric phase: linear and cubic Dirac points

The band structure including SOC is of greater interest because the low-energy states mainly arise from the Os-5d orbitals with strong SOC effects. When the SOC is turned on, the band-crossings in the non-ferroelectric $R\bar{3}c$ phase evolve from 1D nodal lines into 0D Dirac points, each with four-fold degeneracy. Fig. 3(a) shows that close

to Fermi level, now we have a linear Dirac node at each L point (there are three inequivalent L points in the BZ) [Fig. 3(c) and Fig. 4(a,b)]. The original eight-fold degeneracy at T splits under SOC into two Dirac points, where one is linear [Fig. 3(d)] and the other is cubic [Fig. 3(e) and Fig. 4(d,e)]. Hence, we may call this phase as a multi-type Dirac semimetal.

The cubic Dirac point, around which the dispersion is linear along one direction (k_z-axis) and cubic along the other two directions, has been rarely reported in real materials[70]. In previous work, it was believed that such a Dirac point can only appear on a sixfold axis[70,71] and is possible only for two space groups (No. 176 and No. 192)[70]. Our results clearly demonstrate that it can also occur on a threefold axis in the presence of the additional nonsymmorphic (glide mirror) symmetry. In the following, we shall show that the cubic Dirac point is indeed protected by the glide mirror together with the symmorphic crystal symmetries.
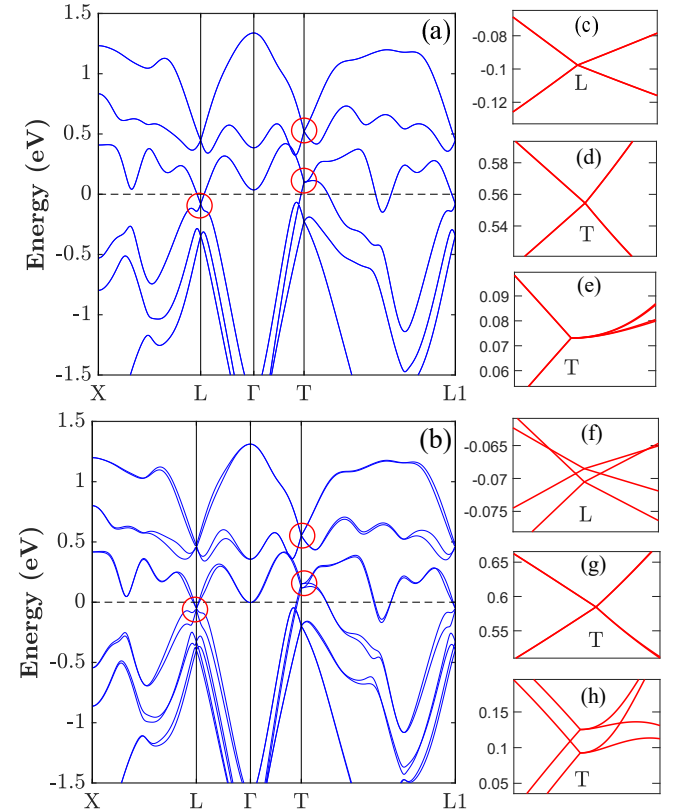

FIG. 3: Electronic band structure for (a) the non-ferroelectric phase and (b) the ferroelectric phase where SOC is included. (c)-(h) Zoom-in images of the band crossings at the L and T points marked by red circles in (a) and (b).

The following points may be noted in connection with symmetry considerations. (1) In the non-ferroelectric phase, the presence of both $\mathcal{T}$ and $\mathcal{P}$ symmetries forces the two-fold spin-degeneracy of each band. Hence the crossing between the bands must be at least 4-fold degenerate (i.e. Dirac type). (2) All states at T and L symme-
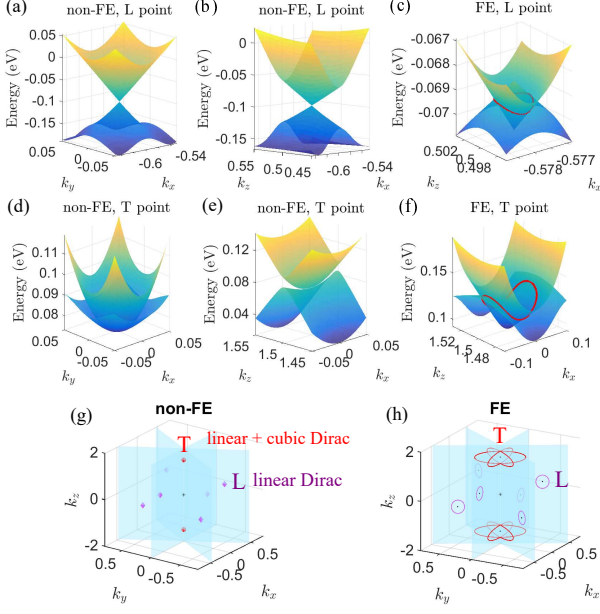
FIG. 4: Top and middle panels show the dispersions around the L and T points. (a), (b), (d) and (e) are for the non-ferroelectric phase, while (c) and (f) are for the ferroelectric phase. (g, h) Schematic diagrams showing the band-crossings in the non-ferroelectric (g) and ferroelectric (h) phases.

try points must be degenerate quadruplets. This reason is that Kramers degeneracy at TRIM points requires the eigenvalues of $\mathcal{P}$ to be paired as $(1,1)$ or $(-1,-1)$. In contrast, at T and L,

$$[\mathcal{P}, \widetilde{M}_y] \neq 0, \tag{2}$$

implying that the degenerate states generated by $\widetilde{M}_y$ will have $\mathcal{P}$ eigenvalues paired as $(1,-1)$, which guarantees the four-fold degeneracy at T and L points. (3) The nature of the Dirac point (linear or cubic) strongly relies on the additional rotational symmetry C_{3z}, which is present at T but not at L, as we will explicitly demonstrate below.

As we already pointed out, the low-energy bands are mainly derived from the Os-$5d$ orbitals. Under trigonal prismatic coordination, the Os d-orbitals split into two groups: A_{1g} (d_{z^2}) and E_g $\{(d_{x^2-y^2}, d_{xy}), (d_{xz}, d_{yz})\}$. Under SOC, these states can be combined into the following spin-orbit-coupled symmetry-adapted basis, keeping in mind that each unit cell contains two Os atoms, one in each sublattice:

$$\phi_{0,s}^{\tau} = |d_{z^2,s}^{\tau}\rangle, \tag{3}$$

$$\phi_{\pm,s}^{\tau} = \frac{1}{\sqrt{2}}(\sin\lambda|d_{xz,s}^{\tau} \pm isd_{yz,s}^{\tau}\rangle + \cos\lambda|d_{x^2-y^2,s}^{\tau} \mp is2d_{xy,s}^{\tau}\rangle), \tag{4}$$

where τ labels the two sublattices A and B, s labels the spin, and λ is a normalization coefficient.

At the T point, Kramers degeneracy requires that the four basis functions $\phi_{i,s}^{\tau}$ with a fixed $i = 0, \pm$ are coupled together into a quadruplet. Consider first the two quadruplet basis $\Psi_{0/-} = (\phi_{0/-,\uparrow}^{A}, \phi_{0/-,\downarrow}^{A}, \phi_{0/-,\uparrow}^{B}, \phi_{0/-,\downarrow}^{B})$, for which the symmetry operations at T take the following representations:

$$\mathcal{T} = -\tau_3 \otimes s_2 K, \quad \mathcal{P} = -\tau_2,$$
$$\widetilde{M}_y = e^{-iq_z/2}\tau_1 \otimes s_2, \quad C_{3z} = \tau_0 \otimes e^{\pm i\frac{\pi}{3}s_3}. \tag{5}$$

Here τ and s are Pauli matrices acting on the sublattice and spin spaces, respectively, and $\boldsymbol{q}$ is the wave-vector measured from T. These expressions fix the $k \cdot p$ Hamiltonian at T expressed using Γ matrices, which we define here as $\gamma^1 = \tau_3 s_1$, $\gamma^2 = \tau_3 s_2$, $\gamma^3 = \tau_1 s_0$, $\gamma^4 = \tau_2 s_0$, and $\gamma^5 = \tau_3 s_3$. Then, to the lowest order, we find that

$$\mathcal{H}_T^{\text{linear}}(\boldsymbol{q}) = \alpha_1(q_x\gamma^1 \pm q_y\gamma^2) + \alpha_2 q_z\gamma^3 + \alpha_3 q_z\gamma^5, \tag{6}$$

where α's are the expansion coefficients, and the sign $\pm$ is for the two basis $\Psi_{0/-}$. This model describes the linear Dirac points at T, which can be viewed as consisting of two Weyl points with Chern numbers 1 and -1. As expected, the total Chern number for a closed surface surrounding the Dirac points vanishes.

As for the other quadruplet basis, $\Psi_+ = (\phi_{+,\uparrow}^{A}, \phi_{+,\downarrow}^{A}, \phi_{+,\uparrow}^{B}, \phi_{+,\downarrow}^{B})$, the representations of the symmetry operations are the same as in Eq. (5) except that $C_{3z} = -\tau_0 \otimes s_0$. Due to this different transformation behavior of the basis under C_{3z}, the related effective Hamiltonian is different from (6), where the diagonal terms proportional to $\tau_0 s_0$ have been dropped:

$$\mathcal{H}_T^{\text{cubic}}(\boldsymbol{q}) = \begin{pmatrix} h_{11} & h_{12} \\ h_{12}^{\dagger} & -h_{11} \end{pmatrix}, \tag{7}$$

where

$$\begin{aligned} h_{11} &= [c_1(q_+^3 + q_-^3) + b_1(q_+q_-q_z) + a_1q_z]s_1 \\ &\quad + ic_2(q_+^3 - q_-^3)s_2 \\ &\quad + [c_3(q_+^3 + q_-^3) + b_2(q_+q_-q_z) + a_2q_z]s_3, \\ h_{12} &= [c_4(q_+^3 + q_-^3) + b_3(q_+q_-q_z) + a_3q_z]s_0. \end{aligned}$$

Here $q_{\pm} = q_x \pm iq_y$, and a_i, b_i, and c_i are the expansion coefficients. We find that the band-crossing at T described by Eq. (7) to be a cubic Dirac point, with cubic dispersion in the q_x-q_y plane. The diagonal blocks describe two triple-Weyl fermions with Chern numbers ± 3. The cubic Dirac point can be viewed as being composed of the two triple-Weyl points.

We emphasize that when only symmorphic symmetries are considered, cubic Dirac points require the presence of a six-fold axis. [70,71] Our case, however, involves a nonsymmorphic glide mirror, which plays a crucial role in realizing the cubic Dirac point on a three-fold axis. Our analysis indicates that a sufficient condition for realizing a cubic Dirac point is the presence of P, T, a glide mirror, and a c3-axis within the mirror. P, T, and the glide
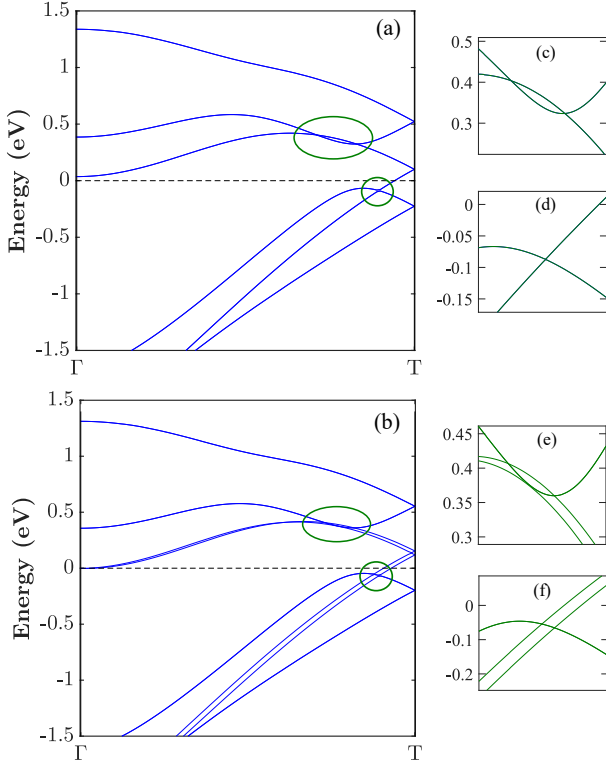
FIG. 5: Accidental band crossing points along the Γ-T symmetry line. (a) Band structure with SOC for the non-ferroelectric phase. (b) Band structure with SOC for the ferroelectric phase. (c,d) Zoom-in images of the band-crossing points marked by green circles in (a). (e,f) Zoom-in images of the band-crossing points in (b). Each band in (c,d) is two-fold degenerate, so that the crossing points are four-fold degenerate. The crossing points in (e,f) lie between a non-degenerate and a two-fold degenerate band, so that these points are triply degenerate.

mirror only protect a four-fold degeneracy; the presence of an additional three-fold rotation then yields the cubic in-plane dispersion.

A similar analysis for the L point at $(0, 0, \frac{1}{2})$ leads to the following effective Hamiltonian:

$$\mathcal{H}_{\mathrm{L}}(\boldsymbol{q}) = \sum_{i=1,3,5} (\beta_{x,i} q_x + \beta_{z,i} q_z) \gamma^i + \beta_y q_y \gamma^2. \qquad (8)$$

Here $\boldsymbol{q}$ is measured from L, and the β's are the expansion coefficients. This demonstrates that the crossings at L are linear Dirac points.

The linear and cubic Dirac points discussed above are *essential* in the sense that their appearance at the high-symmetry TRIM points T and L is mandated by the symmetry operations of the system. In addition, we note the presence of accidental Dirac points, which appear in pairs along the primary rotation axis Γ-T. There are three such pairs around the Fermi level, one of these is seen to be of type-II with an over-tilted dispersion. Zoom-in images of these Dirac points are shown in Figs. 5(a,c,d).

B. Ferroelectric phase: crossed nodal rings

In going across the ferroelectric $R3c$ phase transition, the loss of inversion symmetry induces profound changes in the band structure, see Fig. 3(b). The spin-degeneracy of the bands gets lifted, and the Dirac points in the non-ferroelectric phase become unstable. We find that each linear Dirac point at L develops into a nodal ring on the glide mirror plane, which encloses the L point [Figs. 3(f) and 4(c)]. Also, the cubic Dirac point at T is transformed into three mutually-crossed nodal rings, each lying on a glide mirror plane [Figs. 3(h) and 4(f)]. This topological phase may thus be called a crossed-nodal-ring semimetal. The transformations of these band-crossings across the phase transition are illustrated in Fig. 4(g,h).

The occurrence of the preceding nodal rings in the band structure is also essential in that it is solely determined by symmetry considerations. Note that the glide eigenvalues are $\pm i$ at $\Gamma_1 \in \{\Gamma, X\}$, and ± 1 at $\Gamma_2 \in \{T, L\}$. The presence of $\mathcal{T}$ here requires that the Kramers pairs at the above TRIM points carry complex-conjugated eigenvalues, *i.e.* $(i, -i)$ at Γ_1; and $(1, 1)$ or $(-1, -1)$ at Γ_2. Hence, along any path connecting Γ_1 and Γ_2 in the glide plane, the evolution of the glide eigenvalues drives a switching of Kramers partners. During this switching, two bands with opposite glide eigenvalues must produce a crossing. As this argument holds for any in-plane path, a nodal loop separating Γ_1 and Γ_2 must appear. This symmetry analysis highlights the importance of the nonsymmorphic glide mirror in producing these essential band-crossings.

The transformations described above can also be captured in the effective models. For example, at the T point, starting from the model of Eq. 7 for the cubic Dirac point, the leading order perturbation $\delta \tau_1 s_2$ when the $\mathcal{P}$ is broken, so that a minimal model may be expressed as

$$\mathcal{H}_{\mathrm{T}}^{\mathrm{CNR}}(\boldsymbol{q}) = \mathcal{H}_{\mathrm{T}}^{\mathrm{cubic}}(\boldsymbol{q}) + \delta \tau_1 s_2. \qquad (9)$$

It is straightforward to verify that this model gives three mutually-crossed nodal rings like the DFT calculations. Similarly, the nodal ring around the L point can be derived from the model of Eq. 8 as follows

$$\mathcal{H}_{\mathrm{L}}^{\mathrm{NR}}(\boldsymbol{q}) = \mathcal{H}_{\mathrm{L}}(\boldsymbol{q}) + \delta' \tau_1 s_2. \qquad (10)$$

Note that the linear Dirac points at T are still preserved [Figs. 3(g)], which can be attributed to the non-commutativity of C_{3z} and $\widetilde{M}_y$ in the corresponding basis. The three pairs of accidental Dirac points residing on the primary rotational axis are, however, turned into triply-degenerate nodes as shown in Fig. 5(b,e,f).

Unlike Weyl points, the essential Dirac points may or may not give rise to nontrivial surface states[71]. In Fig. 6, we plot the surface spectrum of the (111)-surface for both the non-ferroelectric and ferroelectric phases. Both phases are seen to support surface bands connecting the two surface-projected L points.
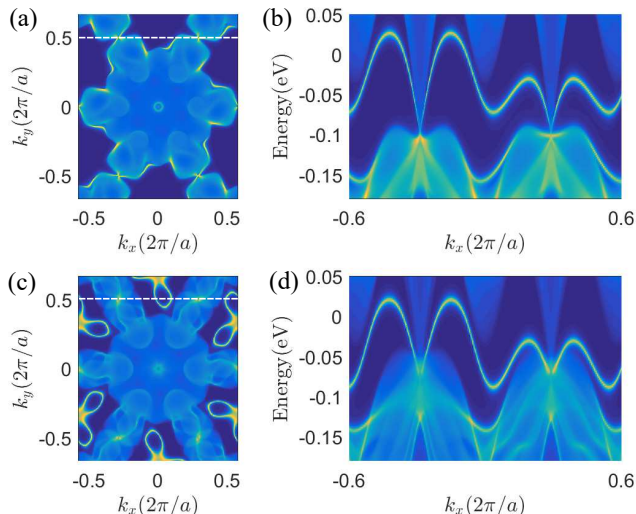
FIG. 6: Surface states of $LiOsO_3$ in the non-ferroelectric (upper panel) and ferroelectric (lower panel) phases in the projected spectra of the (111) surface. SOC is included. (a) and (c) Constant energy surfaces at the band-crossing energy at L. (d) and (e) Dispersions along the k_x-direction at $k_y = 0.5$.

VI. CONCLUSION

We emphasize a number of points in closing. Firstly, the Dirac nodes at the TRIM points and the multiple nodal rings surrounding these points discussed here are *essential* band-crossings in the sense that the presence of these features is solely dictated by the nonsymmorphic space group symmetries (plus $\mathcal{T}$) of the system. Their existence is thus guaranteed as long as these symmetries are preserved. Our analysis of symmetry considerations underlying cubic Dirac points and crossed nodal rings will provide a useful guide in searching for exotic band crossings in realistic material systems more generally.

Secondly, our analysis clearly indicates that $LiOsO_3$ will provide a useful platform for exploring exotic topological phases and their interplay with ferroelectric ordering. The unique advantages of $LiOsO_3$ are as follows. (i) The essential band-crossings are close to the Fermi level, so that the associated topological physics will be reflected in various electronic properties. (ii) The two topological phases that coexist in the same material are connected via a ferroelectric phase transition, which is tunable by varying temperature[73]. And, (iii) the material has already been realized experimentally and its ferroelectric phase transition has been observed. The in-

teresting transformations in the band-crossings across the phase transition, which we have predicted here, could be detected by ARPES experiments.

Thirdly, we have identified the first case of an experimentally realized material, which harbors a cubic Dirac point in a 3D material. Such a Dirac point has been predicted previously only in quasi-1D molybdenum monochalcogenide compounds[70], where an experimental verification is still lacking. Our work offers a new route for realizing cubic Dirac points, extending the range of materials in search of cubic Dirac fermions.

Finally, our study opens a new pathway for exploring a variety of novel effects associated with the various nontrivial band-crossings. For example, a linear Dirac point may exhibit negative magnetoresistance[84,85], a special magnetic oscillation frequency driven by surface Fermi arcs[86], and an artificial gravity field via strain modulation[87]. A cubic Dirac point can exhibit unusual quantum interference contributions to magneto-transport[88], stronger screening of interactions, and possible presence of continuous quantum phase transitions driven by interactions[89]. A nodal ring may yield strong anisotropy in electrical transport[47], unusual optical response[90] and circular dichroism[91], and possible surface magnetism and superconductivity[92].

† Electronic address: physxtzhou@gmail.com
‡ Electronic address: shengyuan_yang@sutd.edu.sg
§ Electronic address: nilnish@gmail.com
[1] A. Bansil, H. Lin, and T. Das, Rev. Mod. Phys. **88**, 021004(2016).

[2] X. L. Qi and S. C. Zhang, Rev. Mod. Phys. **83**, 1057 (2011).
[3] M. Z. Hasan and C. L. Kane, Rev. Mod. Phys. **82**, 3045 (2010).
[4] B. Yan and C. Felser, Annu. Rev. Condens. Matter Phys. **8**, 337 (2017).

[5] Kane, C. L., and E. J. Mele, Phys. Rev. Lett. **95**, 226801 (2005).

[6] Kane, C. L., and E. J. Mele, Phys. Rev. Lett. **95**, 146802 (2005).

[7] B. A. Bernevig, T. L. Hughes, and S. C. Zhang, Science **314**, 1757 (2006).

[8] L. Fu, C. L. Kane, and E. J. Mele, Phys. Rev. Lett. **98**, 106803 (2007).

[9] J. E. Moore, and L. Balents, Phys. Rev. B **75**, 121306 (2007).

[10] R. Roy, Phys. Rev. B **79**, 195322 (2009).

[11] M. Konig, S. Wiedmann, C. Brune, A. Roth, H. Buhmann, L.W. Molenkamp, X.-L. Qi, and S.-C. Zhang, Science **318**, 766 (2007).

[12] D. Hsieh, D. Qian, L. Wray, Y. Xia, Y. S. Hor, R. J. Cava, and M. Z. Hasan, Nature (London) **452**, 970 (2008).

[13] D. Hsieh *et al.*, Nature (London) **460**, 1101 (2009).

[14] D. Hsieh *et al.*, Phys. Rev. Lett. **103**, 146401 (2009).

[15] Y. L. Chen *et al.*, Science **325**, 178 (2009).

[16] Y. Xia *et al.*, Nat. Phys. **5**, 398 (2009).

[17] A. P. Schnyder, S. Ryu, A. Furusaki, and A. W. W. Ludwig, Phys. Rev. B **78**, 195125(2008).

[18] A. Kitaev, AIP Conf. Proc. **1134**, 22 (2008).

[19] S. B. Chung, and S. C. Zhang, Phys. Rev. Lett. **103**, 235301 (2009).

[20] X. L. Qi, T. L. Hughes, S. Raghu, and S.-C. Zhang, Phys. Rev. Lett. **102**, 187001 (2009).

[21] H. Zhang, C.-X. Liu, X.-L. Qi, X. Dai, Z. Fang, and S.-C. Zhang, Nature Phys. **5**, 438 (2009).

[22] L. Fu and C. L. Kane, Phys. Rev. Lett. **100**, 096407 (2008).

[23] X. L. Qi, T. L. Hughes, and S.-C. Zhang, Phys. Rev. B **82**, 184516 (2010).

[24] L. Santos, T. Neupert, C. Chamon, and C. Mudry, Phys. Rev. B **81**, 184502 (2010).

[25] J. D. Sau, R. M. Lutchyn, S. Tewari, and S. Das Sarma, Phys. Rev. Lett. **104**, 040502 (2010).

[26] A. Das *et al.*, Nature Phy. **8**, 887 (2012).

[27] S. A. Yang, H. Pan, and F. Zhang, Phys. Rev. Lett. **113**, 046401 (2014).

[28] M. Z. Hasan, S.-Y. Xu, and G. Bian, Phys. Scripta **2015**, 014001 (2015).

[29] L. Balents, Physics **4**, 36 (2011).

[30] A. M. Turner and A. Vishwanath, *Beyond band insulators: Topology of semimetals and interacting phases* (Elsevier, New York, 2013).

[31] S. A. Yang, SPIN **6**, 1640003 (2016).

[32] C. Fang, H. Weng, X. Dai, and Z. Fang, Chin. Phys. B **25**, 117106 (2016).

[33] A. A. Burkov, arXiv:1704.06660.

[34] S. M. Young, S. Zaheer, J. C. Y. Teo, C. L. Kane, E. J. Mele, and A. M. Rappe, Phys. Rev. Lett. **108**, 140405 (2012).

[35] Z. Wang, Y. Sun, X.-Q. Chen, C. Franchini, G. Xu, H. Weng, X. Dai, and Z. Fang, Phys. Rev. B **85**, 195320 (2012).

[36] Z. Wang, H. Weng, Q. Wu, X. Dai, and Z. Fang, Phys. Rev. B **88**, 125427 (2013).

[37] Z. K. Liu, B. Zhou, Y. Zhang, Z. J. Wang, H. M. Weng, D. Prabhakaran, S.-K. Mo, Z. X. Shen, Z. Fang, X. Dai, Z. Hussain, and Y. L. Chen, Science **343**, 864 (2014).

[38] T. R. Chang *et al.*, Phys. Rev. Lett. **119**, 026404 (2017).

[39] X. Wan, A. M. Turner, A. Vishwanath, and S. Y. Savrasov, Phys. Rev. B **83**, 205101 (2011).

[40] B. Singh, A. Sharma, H. Lin, M. Z. Hasan, R. Prasad, and A. Bansil, Phys. Rev. B **86**, 115208 (2012).

[41] H. Weng, C. Fang, Z. Fang, B. A. Bernevig, and X. Dai, Phys. Rev. X **5**, 011029 (2015).

[42] S.-M. Huang, S.-Y. Xu, I. Belopolski, C.-C. Lee, G. Chang, B. Wang, N. Alidoust, G. Bian, M. Neupane, C. Zhang, S. Jia, A. Bansil, H. Lin, and M. Z. Hasan, Nat. Commun. **6**, 7373 (2015).

[43] A. A. Burkov, M. D. Hook, and L. Balents, Phys. Rev. B **84**, 235126 (2011).

[44] M. Phillips and V. Aji, Phys. Rev. B **90**, 115111 (2014).

[45] C.-K. Chiu and A. P. Schnyder, Phys. Rev. B **90**, 205136 (2014).

[46] H. Weng, Y. Liang, Q. Xu, R. Yu, Z. Fang, X. Dai, and Y. Kawazoe, Phys. Rev. B **92**, 045108 (2015)

[47] K. Mullen, B. Uchoa, and D. T. Glatzhofer, Phys. Rev. Lett. **115**, 026403 (2015).

[48] Y. Chen, Y. Xie, S. A. Yang, H. Pan, F. Zhang, M. L. Cohen, and S. Zhang, Nano Lett. **15**, 6974 (2015).

[49] C. Fang, Y. Chen, H.-Y. Kee, and L. Fu, Phys. Rev. B **92**, 081201 (2015).

[50] R. Yu, H. Weng, Z. Fang, X. Dai, and X. Hu, Phys. Rev. Lett. **115**, 036807 (2015).

[51] Y. Kim, B. J. Wieder, C. L. Kane, and A. M. Rappe, Phys. Rev. Lett. **115**, 036806 (2015).

[52] R. Li, H. Ma, X. Cheng, S. Wang, D. Li, Z. Zhang, Y. Li, and X.-Q. Chen, Phys. Rev. Lett. **117**, 096401 (2016).

[53] S. Li, Z.-M. Yu, Y. Liu, S. Guan, S.-S. Wang, X. Zhang, Y. Yao, and S. A. Yang, Phys. Rev. B **96**, 081106 (2017).

[54] Y. Chen, H.-S. Kim, and H.-Y. Kee, Phys. Rev. B **93**, 155140 (2016).

[55] S. Li, Y. Liu, S.-S. Wang, Z.-M. Yu, S. Guan, X.-L. Sheng, Y. Yao, and S. A. Yang, Phys. Rev. B **97**, 045131 (2018).

[56] T. Bzdusek, Q. Wu, A. Ruegg, M. Sigrist, and A. A. Soluyanov, Nature **538**, 75 (2016).

[57] S.-S. Wang, Y. Liu, Z.-M. Yu, X.-L. Sheng, and S. A. Yang, Nat. Commun. **8**, 1844 (2017).

[58] M. Zeng, C. Fang, G. Chang, Y.-A. Chen, T. Hsieh, A. Bansil, H. Lin, and L. Fu, arXiv:1504.03492.

[59] S. Kobayashi, Y. Yamakawa, A. Yamakage, T. Inohara, Y. Okamoto, and Y. Tanaka, Phys. Rev. B **95**, 245208 (2017).

[60] X.-L. Sheng, Z.-M. Yu, R. Yu, H. Weng, and S. A. Yang, J. Phys. Chem. Lett. **8**, 3506 (2017).

[61] G. Chang, S.-Y. Xu, X. Zhou, S.-M. Huang, B. Singh, B. Wang, I. Belopolski, J. Yin, S. Zhang, A. Bansil, H. Lin, and M. Z. Hasan, Phys. Rev. Lett. **119**, 156401 (2017).

[62] C. Zhong, Y. Chen, Z.-M. Yu, Y. Xie, H. Wang, S. A. Yang, and S. Zhang, Nat. Commun. **8**, 15641 (2017).

[63] W. Chen, H.-Z. Lu, and J.-M. Hou, Phys. Rev. B **96**, 041102 (2017).

[64] Z. Yan, R. Bi, H. Shen, L. Lu, S.-C. Zhang, and Z. Wang, Phys. Rev. B **96**, 041103 (2017).

[65] P.-Y. Chang and C.-H. Yee, Phys. Rev. B **96**, 081114 (2017).

[66] M. Ezawa, Phys. Rev. B **96**, 041202 (2017).

[67] Z. Wang, A. Alexandradinata, R. J. Cava, and B. A. Bernevig, Nature **532**, 189 (2016).

[68] S. M. Young and C. L. Kane, Phys. Rev. Lett. **115**, 126803 (2015).

[69] S. Guan, Y. Liu, Z.-M. Yu, S.-S. Wang, Y. Yao, and S. A. Yang, Phys. Rev. Materials **1**, 054003 (2017).

[70] Q. Liu and A. Zunger, Phys. Rev. X **7**, 021019 (2017).

[71] B.-J. Yang and N. Nagaosa, Nat. Commun. **5**, 4898 (2014).

[72] P. W. Anderson and E. I. Blount, Phys. Rev. Lett. **14**, 217 (1965); Phys. Rev. Lett. **14**, 532(1965).

[73] Y. Shi et al., Nat. Mater. **12**, 1024 (2013).

[74] R. Li, Y. Xu, J. He, S. Ullah, J. Li, J.-M. Liu, D. Li, C. Franchini, H. Weng, and X.-Q. Chen, arXiv:1610.07142.

[75] K. Schwarz and P. Blaha, Comput. Mater. Sci. **28**, 259 (2003).

[76] J. Perdew, K. Burke, and M. Ernzerhof, Phys. Rev. Lett. **77**, 3865 (1996).

[77] A. H. MacDonald, W. E. Pickett, and D. D. Koelling, J. Phys. C: Solid State Phys. **13**, 2675 (1980).

[78] A. A. Mostofi, J. R. Yates, G. Pizzi, Y. S. Lee, I. Souza, D. Vanderbilt, and N. Marzari, Comput. Phys. Commun. **185**, 2309(2014)

[79] N. Marzari and D. Vanderbilt, Phys. Rev. B **56**, 22(1997).

[80] I. Souza, N. Marzari, and D. Vanderbilt, Phys. Rev. B **65**, 035109 (2001).

[81] N. Marzari, A. A. Mostofi, J. R. Yates, I. Souza, and D. Vanderbilt, Rev. Mod. Phys. **84**, 1419 (2012)

[82] J. Kuneš, R. Arita, P. Wissgott, A. Toschi, H. Ikeda, and K. Held, Comput. Phys. Commun. **181**, 1888 (2010).

[83] M. P. L. Sancho, J. M. L. Sancho, J. Rubio, J. Phys. F Met. Phys. **15**, 851(2000).

[84] J. Xiong, S. K. Kushwaha, T. Liang, J. W. Krizan, M. Hirschberger, W. Wang, R. Cava, and N. P. Ong, Science **350**, 413 (2015).

[85] Y. Gao, S. A. Yang, and Q. Niu, Phys. Rev. B **95**, 165135 (2017).

[86] P. J. W. Moll, N. L. Nair, T. Helm, A. C. Potter, I. Kimchi, A. Vishwanath, and J. G. Analytis, Nature **535**, 266 (2016).

[87] S. Guan, Z.-M. Yu, Y. Liu, G.-B. Liu, L. Dong, Y. Lu, Y. Yao, and S. A. Yang, npj Quantum Materials **2**, 23 (2017).

[88] X. Dai, H.-Z. Lu, S.-Q. Shen, and H. Yao, Phys. Rev. B **93**, 161110 (2016).

[89] B. Roy, P. Gaswami, and V. Juričić, Phys. Rev. B **95**, 201102 (2017).

[90] S. Ahn, E. J. Mele, and H. Min, Phys. Rev. Lett. **119**, 147402 (2017).

[91] Y. Liu, S. A. Yang, and F. Zhang, Phys. Rev. B **97**, 035153 (2018).

[92] T. T. Heikkila and G. E. Volovik, JETP Lett. **93**, 59 (2011).